JOURNAL OF AIRCRAFT
Vol. 38, No. 6, November–December 2001

Experimental Validation of the Wing Dihedral Effect Using a Whirling Arm Equipment

Piero A. Gili* and Manuela Battipede†
Politecnico di Torino, 10129 Torino, Italy

By the use of whirling arm equipment, tests have been carried out on a wing model equipped with a suitable strain-gauge balance. The purpose of this work was to verify analogous theoretic results from the dihedral effect trends (C_{l_β} derivative), which were detected on a wing with generic geometry. Full details are put forward concerning the remarkable possibilities that this system offers for the experimental determination of all main aerodynamic derivatives in the state variables within the aircraft dynamics equations. The experimental facility induces a test situation, which calls for careful and in-depth result processing in addition to the normal corrections arising from Reynolds and Mach numbers. The results, presented as theoretical–experimental comparisons, strongly support the theoretic calculation.

Nomenclature

AR	=	aspect ratio
a.c.$_w$	=	wing aerodynamic center
b	=	wing span
c.g.	=	center of gravity
C_i	=	generic coefficient
C_{L_α}	=	wing lift coefficient-curve slope
C_l	=	rolling moment coefficient
C_{l_α}	=	section lift coefficient-curve slope
C_{l_β}	=	dihedral effect, $\partial C_l/\partial\beta$
C_n	=	yawing moment coefficient
c_m	=	mean geometric chord
c_r	=	wing root chord
c_t	=	wing tip chord
c.v.	=	balance virtual center
F_c	=	centrifugal force
f	=	natural oscillation frequency
L, M, N	=	moments in balance axes (roll, pitch, and yaw)
p, q, r	=	roll, pitch, and yaw rates
R	=	wing taper ratio, c_t/c_r
Re	=	Reynolds number
S	=	wing area
t	=	time
V	=	test speed, V_∞
V'	=	model speed when $\beta \neq 0$ deg
X, Y, Z	=	forces in balance axes
x, y, z	=	balance axes
x', y', z'	=	platforms rotation axes
α	=	wing angle of attack
α_i	=	section induced angle of attack
$\dot{\alpha}$	=	wing angle-of-attack rate
β	=	sideslip angle
β'	=	platform rotation to obtain β
γ	=	dihedral wing angle
δ_a	=	ailerons deflection angle
δ_e	=	elevator deflection angle
δ_r	=	rudder deflection angle
ε	=	twist from root to tip
Λ	=	swept wing angle
ρ	=	air density
ϕ, θ, ψ	=	Euler angles
Ω	=	whirling arm rotation speed

Subscripts

corr	=	correct
e	=	experimental
h	=	wing horizontal position
i	=	incompressible
p	=	derivative in p
q	=	derivative in q
r	=	derivative in r
t	=	theoric
v	=	wing vertical position
α	=	derivative in α
$\dot{\alpha}$	=	derivative in $\dot{\alpha}$
β	=	derivative in β

Introduction

THE direct forced-oscillation technique in a wind tunnel is the classic method used for the experimental determination of the stability derivatives. Numerous researchers have followed this path for several applications, for example, Beyers[1] applied it to the standard dynamics model and den Boer and Cunningham[2] and Cunningham and den Boer[3] investigated a pitching straked wing. E. S. Hanff[4] of the Unsteady Aerodynamics Laboratory in Ottawa developed this method with several variations on the theme (half-model technique). Several papers illustrate studies of the secondary effects on the model: sting plunging,[5] different frequencies in small-amplitude oscillations,[6] and so on. Reference 7 is a series of results, attained by using this experimental technique in 10 different wind tunnels. A comparison is made with models of a schematic combat aircraft configuration and two generic aircraft forebodies.

The rotating model is another experimental methodology, essentially used for the damping aerodynamic derivatives determination. In Ref. 8, in addition to a survey on the effects of different configurations and the Reynolds number, a comparison is put forward with similar data obtained from small-amplitude oscillatory tests. The state of the art has many papers dealing with different aspects of the rotating model technique. Some authors[9] tackled the problem of interference between the model and the support at high angles of attack by proposing a method to correct these effects. Ericsson[10,11] and Ericsson and Beyers[12] found a satisfactory solution to determine the coupled effects of the subscale Reynolds number and the interference between the model support and the vortex wake shed, for an advanced aircraft model at high angles of attack. In this context, the

Received 21 July 2000; revision received 3 July 2001; accepted for publication 12 July 2001.

*Associate Professor, Dipartimento di Ingegneria Aeronautica e Spaziale, C.so Duca degli Abruzzi 24; gili@polito.it. Member AIAA.

†Ph.D Researcher, Dipartimento di Ingegneria Aeronautica e Spaziale, C.so Duca degli Abruzzi 24; gili@polito.it. Member AIAA.

problem of the simulation of high Reynolds numbers, for combat aircraft models, is also addressed. In Ref. 13, in addition to the support interference and the steady-state hysteresis phenomena, some very interesting results are shown: They highlight the existence of a threshold rotation rate that strongly affects the rotary balance data.

Another technique centers on the superposition of the oscillatory and conning motions; through this experimental rig, it is possible to secure the pure unsteady aerodynamic derivatives.[14] A rotary rig can also be employed to determine the instantaneous asymmetric loads of a full-scale aircraft or a missile.[15]

An alternative to forced oscillations and rotary tests in a wind tunnel for the determination of the aerodynamic derivatives is to use a whirling arm facility.[16] The present authors adopted a similar device to obtain test data for a swept tapered wing.

Likewise, one of this paper's authors was engaged in the theoretical determination of several stability derivatives for lengthily periods and focused much of his attention on an aerodynamic derivative, which is improperly named lateral stability: the dihedral effect C_{l_β}. Applying a modified version of the Anderson method, he proposed a calculation procedure for generic wings (see Refs. 17 and 18). Then he compared[19] this calculation method with another one, still based on the vortex theory, in which the determination of α_i was carried out by means of an iterative process.

The results of this study are laid out in this paper. It began with two principal aims in mind: 1) to validate, using the experimental data, the theoretical results obtained from the aforementioned numerical methods and 2) to present an experimental technique that can be successfully used to evaluate all of the aerodynamic derivatives in the angular speeds p, q, and r and, in particular, to propose an effective procedure for extrapolating data from conditions set by the experimental device to more generic and real conditions.

The basic points of the two theoretic methods will be summarized in the first section. Following is the experimental facility, presented complete with an exhaustive overview on its hypothetical range of application, for the determination of all of the main aerodynamic derivatives. Finally, the procedures for the test data analysis and processing are explained, with close attention to corrections due to Reynolds and Mach numbers, which have remarkable differences in their theoretical and experimental situations.

C_{l_β} Theoretical Determination

The theoretical results, used in the comparison with the experimental ones, are drawn from the aforementioned paper[18] by one of the present authors. The two theoretical methods basically differ in the calculation of α_i, but are both based on the use of the Anderson method.[20] Briefly, we will just recount that this method is based on the Prandtl theory for wings of finite aspect ratio and actually offers an approximate solution of the Prandtl integral-differential equation. The adopted calculation process takes into account the wake vortices circulation effects on the lift coefficient and, therefore, on the rolling moment coefficient. The classic lifting line theory of Prandtl cannot be used for swept and/or no-planar wings. This point was discussed by many authors: for example, the first section of Ref. 21 provides a brief review of the various lifting line theories and their applicability limits. It is clear that the Anderson method offers an approximate solution that increasingly improves as the wing approaches a straight wing and has a high aspect ratio. However, because the final aim is to calculate the C_{l_β}, it is simply the difference of lift between the two semiwings that must be evaluated. It is not necessary to evaluate the real lift of the two semiwings.

A reminiscent of the approach of Ref. 19 can be found in Refs. 22 and 23, dated 1956 and 1968, respectively. Because of limited computational capacity in those years, this kind of approach was certainly preferred to others, such as the vortex lattice method (which was also applied for the determination of the aerodynamic derivatives[24,25]). For the same reasons, other numerical methods, such as the boundary integral method, capable of computing the C_{l_β} derivative, have only been developed in recent years. However, the use of such an obsolete numerical method is not to be totally disregarded. As a matter of fact, the theoretic methodology used for this theoretical–experimental comparison is certainly a simple but useful tool for the evaluation of stability derivatives.

As far as the calculation of the induced angle of attack is concerned, the first method employs the Biot–Savart formula, whereas the second method determines the α_i trend along the wing span through an iterative process. During the first iteration, an initial trend of α_i is fed, from which the new distribution can be calculated. It has been noted how the wing vortex scheme influences the convergence process speed, but the number of the wake vortices does not matter, nor does the vortex core diameter, because the induced speed on a generic wing point is only a function of the actual lift of the wing.

Summarizing, the two calculation methods seem to offer good results: The first one has a lower computing time because it is based on an approximate procedure. From the comparison between the two calculation methods, note that the dihedral effect calculated with the second method is slightly higher than the one calculated with the first method.

Experimental Facility

First, note that the whirling arm equipment was not devised for the experimental purposes in this work (it was created in the 1970s for the calibration of anemometers). It, therefore, has some geometric and cinematic limitations: with a model of size and weight suitable to be assembled on the arm and with the turn rate allowed by the motor, the Reynolds Number is approximately: $Re = 0.5 \times 10^5$.

The whirling arm equipment and its main geometric features are shown in Fig. 1. The rotational speed of the arm is set with negligible errors by a suitable system. The maximum speed at tip arm is 7 m/s (speed of the model).

The model rotational device is sketched in Fig. 2. It consists of three rotating platforms with rotation axes shaping an orthogonal system. The platforms are equipped with step-by-step motors connected to an electronic card, so that movements are managed by computer, like the continuous measurement of the angular position, making it is possible to set the model at the required α and β angles and to move it at the rotation speed p. The rotation of the equipment arm provides the velocity components q and r depending on, respectively, the vertical or horizontal model placing.

The strain-gauge balance is connected to the sting and is contained in the ogive that links the two semiwings of the model (see Fig. 3). It is a six-component balance whose maximum values are on the kilo order for forces and on the hundred grams·meter order for moments.

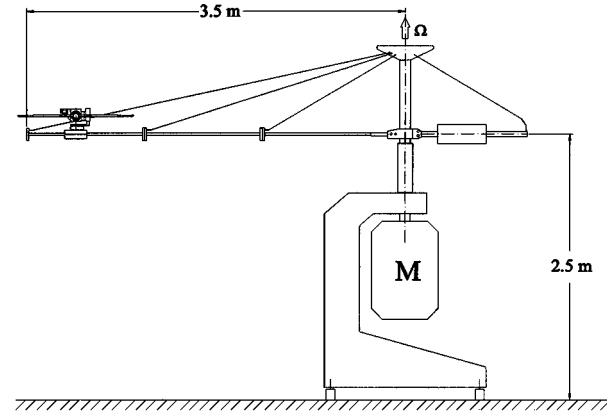

Fig. 1 Whirling arm equipment.

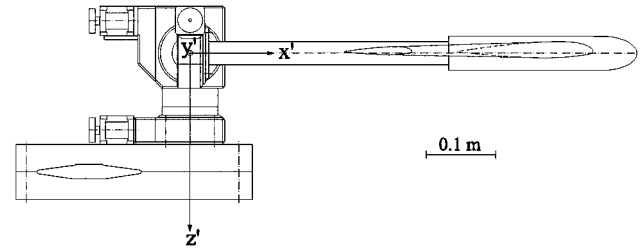

Fig. 2 Model rotational device.

Table 1 Laterodirectional and longitudinal aerodynamic derivatives

Lat-dir	β	p	r	Long	α	$\dot{\alpha}$	q
Y	C_{Y_β}	C_{Y_p}	C_{Y_r}	X	C_{X_α}	$C_{X_{\dot{\alpha}}}$	C_{X_q}
L	C_{l_β}	C_{l_p}	C_{l_r}	Z	C_{Z_α}	$C_{Z_{\dot{\alpha}}}$	C_{Z_q}
N	C_{n_β}	C_{n_p}	C_{n_r}	M	C_{M_α}	$C_{M_{\dot{\alpha}}}$	C_{M_q}

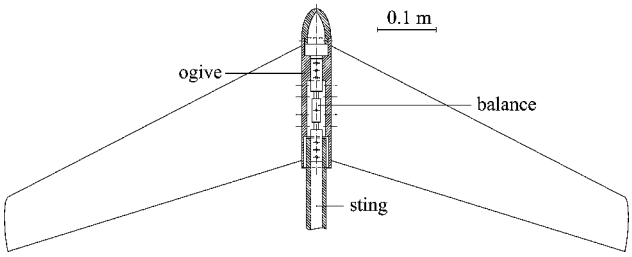

Fig. 3 Model forces measurement and rest device.

Experimental Determination of Aerodynamic Derivatives

Apart from the theoretical–experimental comparison on the C_{l_β} values, the experimental device gives way to an evaluation of all of the main aerodynamic derivatives. Table 1 shows the aerodynamic derivatives that appear in the classic formulation of the linearized motion equations, with separation between longitudinal and laterodirectional motion. This experimental method can also be used to evaluate the aerodynamic coefficients that generally appear in nonlinear aerodynamic models.

With reference to Table 1, the main aerodynamic derivatives can be evaluated as follows:

1) For derivatives in α and β, it is sufficient to perform several tests at different angles to single out the linear part of the aerodynamic characteristic curves.

2) For derivatives in q and r, if $\alpha = 0$ and $\beta = 0$, then the procedure is the same as described for the derivatives in α and β: q and r are varied while the linear trend of the aerodynamic coefficients is verified. In particular, the model is placed in the horizontal position (wing level) to have $r \neq 0$ and $q = 0$, in the vertical position (see Fig. 4) to have $q \neq 0$ and $r = 0$. If $\beta \neq 0$ the derivative in r of the generic coefficient can be obtained as follows:

$$C_{i_r}(\beta) = \left[C_{i_h}(\beta, r) - C_{i_v}(\beta)\right]/\Omega, \qquad i = Y, l, n \quad (1)$$

with $\Omega \equiv r$.

Similarly, if $\alpha \neq 0$, the derivative in q of the generic coefficient is

$$C_{i_q}(\alpha) = \left[C_{i_v}(\alpha, q) - C_{i_h}(\alpha)\right]/\Omega, \qquad i = X, Z, M \quad (2)$$

with $\Omega \equiv q$.

3) Estimating derivatives in p and $\dot{\alpha}$ involves dynamic tests, namely, the model moves in relation to the whirling arm, and, thus, the balance output is likely to experience a measure delay, depending on the degree of unsteadiness. Time delay must be evaluated to select the actual values of the coefficients: For p derivatives, the model rotates around the x' axis and the generic C_{i_p} is measured when $\phi = 90$ deg, that is, $r = 0$. Instead, for $\dot{\alpha}$ derivatives the model oscillates in line with the horizontal position around the y' axis. The generic $C_{i_{\dot{\alpha}}}$ is measured when $\alpha = 0$ deg. The results of this test must be purified from the model's moment of inertia, which affects the balance measure. This can be easily done by moving the model at $V = 0$ with the same $\alpha(t)$ test law and measuring forces and moments in this situation.

Another problem may arise during the tests where the model moves through the whirling arm, for example, in the pitch oscillations for the determination of the $\dot{\alpha}$ derivatives. In these cases, the structural frequencies have to be estimated to impose a proper cutoff frequency in the low-pass filter, during the postprocessing phase. At the same time, the forcing frequency should be maintained far below these values. Free oscillation tests with a still model have been carried out. The damping is very low for all oscillations, and the measured first harmonic natural frequencies are the following:

$$f_{\text{roll}} = 6.7\,\text{Hz}, \qquad f_{\text{pitch}} = 4.2\,\text{Hz}, \qquad f_{\text{yaw}} = 2.2\,\text{Hz}$$

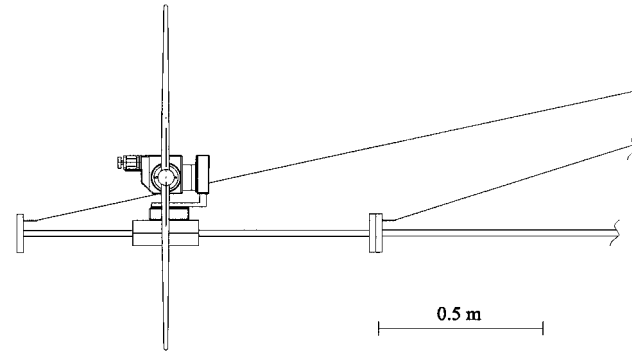

Fig. 4 Wing model vertical position.

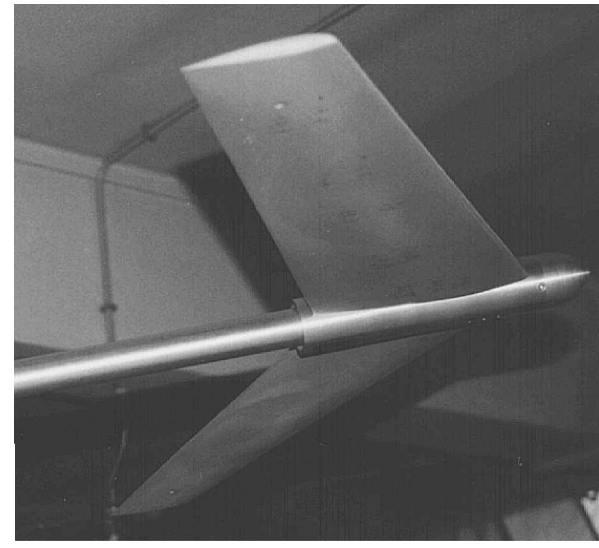

Fig. 5 Wing model during a test.

Model

The wing model (Fig. 5 depicts the model during a test) has constant airfoil NACA 23012 along the span, and, thus, $C_{l_\alpha} = 5.79$, as was assumed in the theoretic calculation. It presents the following main geometrical characteristics:

$$\Lambda = 25\,\text{deg}, \qquad A = 7, \qquad c_m = 150\,\text{mm}$$

$$R = c_t/c_r = 0.5, \qquad b = 1050\,\text{mm}, \qquad \epsilon = 0\,\text{deg}$$

With this aspect ratio, the wing lift coefficient-curve slope is about $C_{L_\alpha} = 4.5$.

In the theoretic determination case, the effects of the variations of the geometric characteristics Λ, γ, R, and ϵ on C_{l_β} had been evaluated. For the test case, only the wing dihedral angle can vary; the two semiwings can be fitted to the ogive in three different positions: $\gamma = 0$, $+10$, and -10 deg. Figure 6 depicts these possible situations and the consequent c.g. positions. These choices were made to have more experimental points to compare with the theoretical results.

Figure 7 shows the internal strain-gauge balance and the ogive that connects the semiwings; the relative position of the characteristic points of the model (c.g., c.v., and a.c._w) are also shown either in Fig. 6 or in Fig. 7.

As far as the c.g. position is concerned, a calibration frame was used to locate the center of gravity of the whole wing–ogive. In

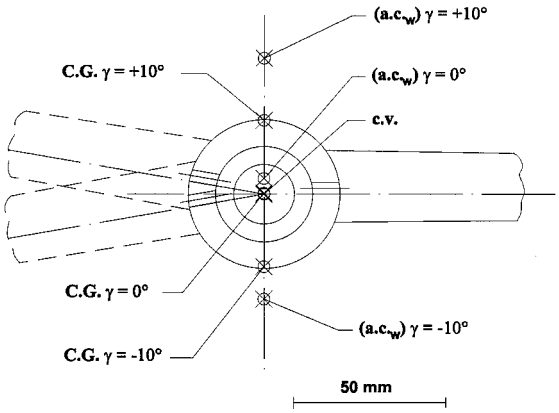

Fig. 6 Different, feasible wing dihedral angles.

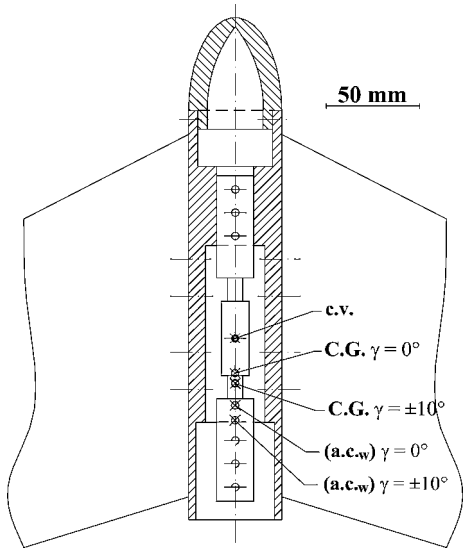

Fig. 7 Longitudinal relative characteristic points position.

the different configurations (different γ) the c.g. position obviously changes: The CAD design already provided these different positions, but, due to possible imperfections in the model construction, the actual positions might be slightly different from the design ones. A static test at the calibration frame provided the resultants of forces and moments measured with respect to the c.v. balance point. Thus, the moment transposition formula allowed the c.g. position to be located.

Experimental Procedure

Two different test sets have been carried out: the first one, by positioning the model horizontally ($\phi = 0$ deg) for different values of α and β, the second one by having the model in vertical position ($\phi = 90$ deg) and the same values of α and β. If the final results of the two test sets coincide, we can ascertain the reliability of the experimental results.

Some phenomena occur during the tests. They must be kept under control to assess their extent and to correct the errors they entail:

1) During the force and moment measurement on the model, oscillations occur in the output voltage of the strain-gauge balance. A typical situation that takes place is the one shown in Figs. 8 and 9, with the overlapping of two main frequencies: one with higher amplitude and low frequency and one with high frequency and much more reduced amplitude (note, however, that the relative amplitude of these oscillations is very small). The lower frequency oscillation is certainly due to the environmental test conditions: The whirling arm equipment is situated in a small room whose dimensions may affect measures during rotation. The higher frequency oscillation is conditioned by the vertical and horizontal oscillations of the whirling

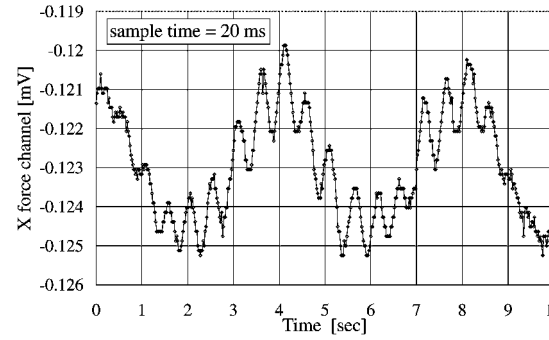

Fig. 8 *X* force output balance time history.

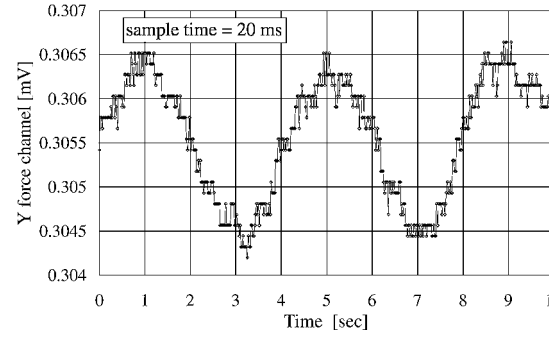

Fig. 9 *Y* force output balance time history.

arm. Although equipped with bars, the whirling arm actually oscillates vertically due to the bending (this natural oscillation of 16 Hz is found in the *Y* force trend of Fig. 9). Furthermore, it oscillates horizontally due to the mechanical drive backlash between the shaft motor and the whirling arm (this second oscillation of 2 Hz is found in the *X* force trend of Fig. 8). These frequencies determine the maximum sample time and the minimum length of each test.

2) The experimental measurement repeatability is a well-known problem. In this case, due to a nonrandom nature in the oscillations of the measured parameters, a high acquisition frequency is appropriate. Also, the acquisition period must be proper, and, in particular, must be a multiple of the longest oscillations period due to the steady aforementioned oscillations. To obtain repeatable results, the authors chose to adopt a sample time of 20 ms with a time test of about 12 s (approximately three turns of the whirling arm at the maximum test speed).

3) Any strain-gauge balance experiences elastic deformations when it is subject to forces and moments. These deformations affect the positioning angles of the model, which means they must be corrected as a function of the loads applied to the model. In this case, static tests revealed that the only deformation of nonnegligible amplitude was the one relevant to the ϕ angle (approximately 3 deg/kgm due to the rolling moment).

4) As shown in Fig. 10 (not drawn to scale), there are two systems of orthogonal axes on the model: (x', y', z') centered in the B point, which is the rotation center of the model rotating system, and (x, y, z) with the origin in the virtual center of the balance c.v., which is a fixed point. Forces and moments refer to this last system; in fact, the balance measures the moments with respect to the c.v. point. It is then sufficient to purge measured forces and moments of the F_c contribution (which is conceived during testing and is obviously applied in the c.g. point), to obtain the actual aerodynamic moments and forces. The $\beta = 0$ deg reference of the wing is bound by setting the symmetry plane of the model perpendicular to the radial direction passing through the c.v. point. From Fig. 10, it is also evident that the platform rotation angle β' is different from the actual sideslip angle β and the model speed is a function of β: namely $V' \neq V$. Note that each point on the longitudinal axis has a different translational speed: c.v. has been chosen as the reference point because it is the balance axes origin. Anyway, at the maximum

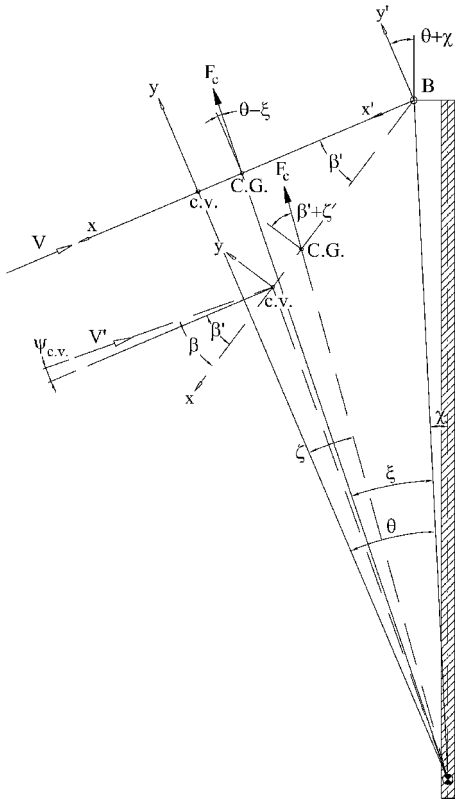

Fig. 10 Plan sketch of the experimental situation.

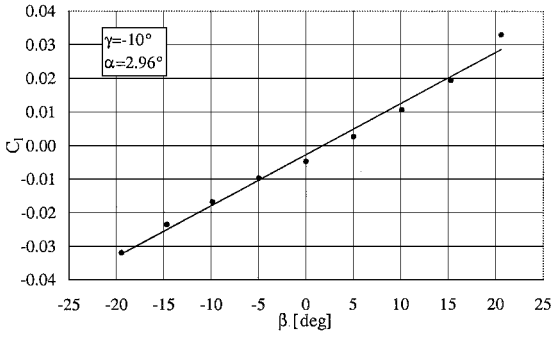

Fig. 11 Rolling moment coefficient as a function of β (low α).

β value (20 deg), the difference between the translational speed of two characteristic extreme points (c.v. and a.c.$_w$) is less than 1%.

5) During tests, an aerodynamic problem arose in the model wake vortices and the wing downwash: Turn after turn, the model covers a trajectory characterized by an environmental situation disturbed by the previous passing. This problem was largely solved by marking areas' boundaries, swept by the whirling arm, with proper pieces of very light and loose weave (about 1 mm) fabric. This expedient turned out to be the best solution in light of the conclusions drawn from a set of thorough tests performed in a previous study.

Experimental Results and Comparison

Figures 11 and 12 show two examples of the C_l trend, as a function of β. As far as small perturbations (small β angles) are concerned, the trend should be linear. The second example, concerning a higher α, shows a trend that differs from the linear one for high, positive β angles. This highlights a problem deriving from a defect in the experimental equipment: In the positive rotation of β, the left wing tip approaches one of the bars of the whirling arm determining an aerodynamic disturbance on the wing, definitely detected by the balance.

From the slope of curves of the type shown in Figs. 11 and 12, the values of C_{l_β} can be found. Figure 13 shows the C_{l_β} trend as

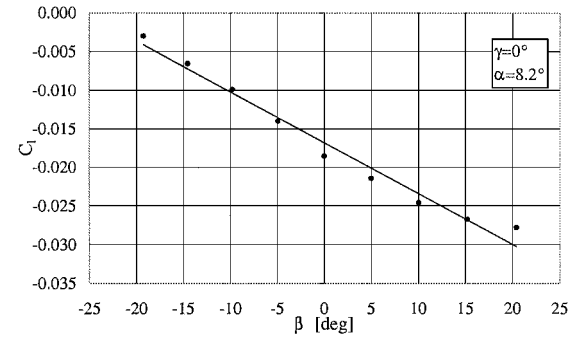

Fig. 12 Rolling moment coefficient as a function of β (high α).

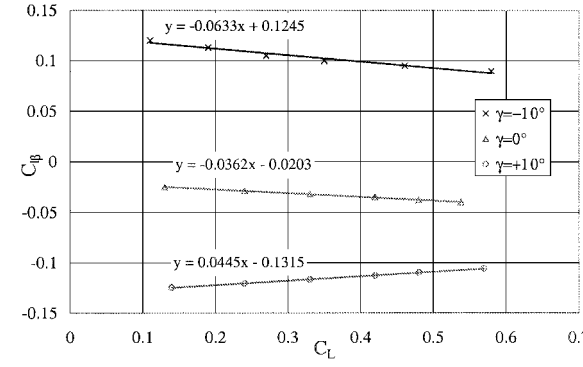

Fig. 13 $C_{l_\beta}(C_L)$ trends for different γ values.

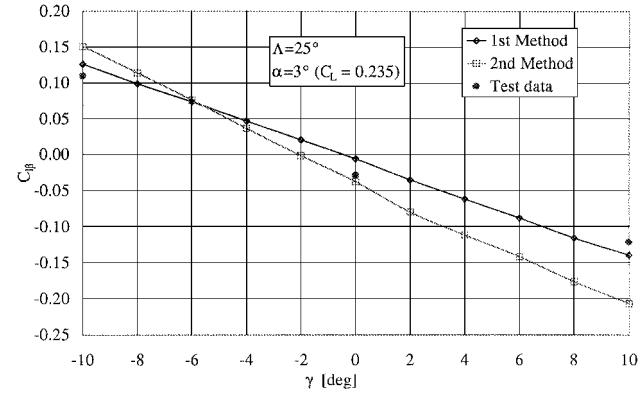

Fig. 14 Experimental–theoretical comparison on C_{l_β} values (low α).

a function of C_L for the three different γ values. Unlike the other wing contributions to C_{l_β} (Λ, different aerodynamic circulation of the two semiwings, etc.), the dihedral angle γ provides a contribution that should not depend on C_L according to simplified theories, (for example, the one of the wing finite element theory). Figure 13 shows that the curve slope changes with γ, also meaning that this contribution actually depends on C_L. This is accounted for because the three-dimensional aerodynamic effects on the wing change as a function of γ when C_L increases.

By means of the curves of Fig. 13, from the abscissa value of the theoretic C_L, we find the value of C_{l_β} to be compared with the theoretical values. This comparison is shown for two values of α in Figs. 14 and 15: For the highest geometric angle of attack ($\alpha = 9$ deg), the experimental–theoretical accordance is not so good.

This discrepancy can be imputed to the effects of Reynolds and Mach numbers, which affect not only the aerodynamic coefficients but also the aerodynamic derivatives.

Effects of Reynolds and Mach Numbers

The Reynolds number adopted for the theory calculation was $Re_t = 3 \times 10^6$, whereas the experimental situation produces

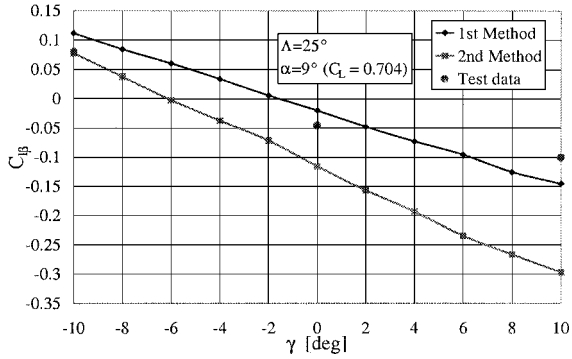

Fig. 15 Experimental–theoretical comparison on C_{l_β} values (high α).

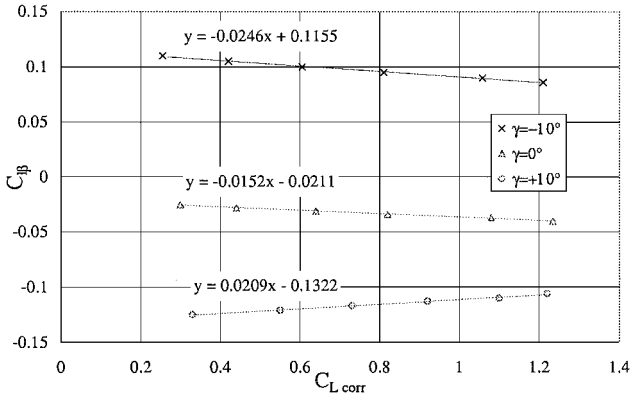

Fig. 16 $C_{l_\beta}(C_{L_{\text{corr}}})$ trends for different γ values (with Reynolds and Mach number corrections).

$Re_e = 0.5 \times 10^5$, namely, there is a difference of two orders of magnitude. Thus, to compare experimental and theoretical results, proper corrections need to be applied. The Reynolds number affects in a direct way mainly the maximum value of the lift coefficient, which is irrelevant in this context, whereas its direct influence on the C_{L_α} value is negligible, unless very low Reynolds numbers are involved. However, to have the experimental Reynolds number equal to the theoretical one, the model speed should be $V = 310$ m/s, corresponding to $M = 0.9$, when it is actually 0.014. Because the Mach number considerably affects the C_{L_α} value, it is necessary to consider the compressibility effects and to apply the corrections on the experimental results, as suggested by the Glauert–Prandtl relation (3), reported, for example, in Ref. 26:

$$C_{L_{\alpha_{\text{corr}}}} \Big/ C_{L_{\alpha_i}} = 1 \Big/ \sqrt{1 - M^2} \tag{3}$$

This correction is applied directly to the wing and defines the C_{L_α} increment with M. From the experimental data C_{L_e} and α_e, we can obtain $C_{L_{\alpha_e}}$, then apply the correction to obtain $C_{L_{\alpha_{\text{corr}}}}$, and finally calculate $C_{Le,\text{corr}} = C_{L_{\alpha\text{corr}}}\alpha_e$. With these correct values of C_L, we can draw the $C_{l_\beta}(C_{L_{\text{corr}}})$ curves of Fig. 16. From the abscissa values of these curves, using the theoretical C_L values, we obtain the C_{l_β} values.

This new comparison is reported in Figs. 17 and 18, for the two values of α. Actually, the experimental–theoretical consistency is improved for both of the α values.

For the experimental point relative to $\gamma = 10$ deg, the shifting from the linear theoretic trend is due to the same aerodynamic interference seen before. When the wing tips are upward, just $\gamma = 10$ deg, disturbance caused by the tension bar is quite evident. In any case, the experimental results do highlight that the first theoretical method, the simplest one, gives better results. Evidently, the second method, which uses an iterative procedure for the induced angle-of-attack calculation, gives some convergence problems. This is rather distinct when high α values are involved.

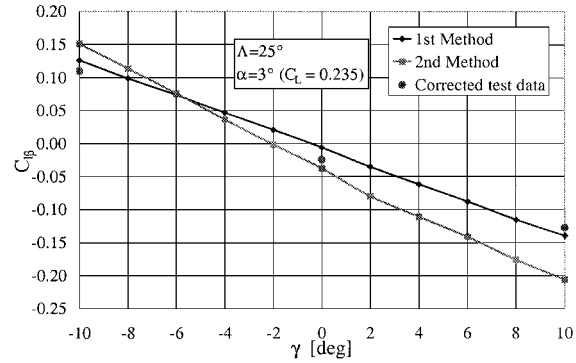

Fig. 17 Experimental–theoretical comparison with Reynolds and Mach number corrections on C_{l_β} values (low α).

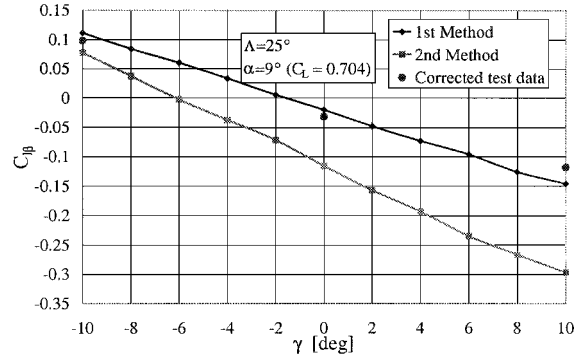

Fig. 18 Experimental–theoretical comparison with Reynolds and Mach number corrections on C_{l_β} values (high α).

Conclusions

A good consistency has been obtained between theoretical and experimental results thanks to using great care when calculating the parasite moments, taking into consideration all possible causes of error, and correcting the effect of different Reynolds and Mach numbers between the theoretical and the experimental situations. On this subject, a method for extrapolating results from very low Reynolds and Mach numbers to those commonly used in aeronautics can be very useful when big and powerful experimental facilities are not available.

Any experimental device for the measurement of aerodynamic derivatives may have design problems, and perhaps a whirling arm system has fewer problems than the others. The versatility of this system for the determination of aerodynamic derivatives is certainly higher than the other commonly employed systems. For example, with forced-oscillation techniques, only a few stability and damping derivatives can be measured, whereas the model-rotating techniques are suitable only for a few damping and cross derivatives. Instead, the whirling arm system enables tests for the determination of all of the main aerodynamic coefficients and derivatives.

The experimental plant is simpler, owing to the model-moving system, and, moreover, with a complete aircraft model, purposely equipped with movable control surfaces, it is also possible to measure special maneuver derivatives (and, therefore, measure derivatives in δ_a, δ_e, δ_r, and so on) or aerodynamic derivatives in turning flight by positioning the model with suitable bank angles.

Finally, we can say than even a small-scale piece of equipment, like the one illustrated in this work, can prove to be very useful in aeronautics. Mach and Reynolds number corrections can be carried out, as noted, when necessary, notwithstanding that cases do exist where these corrections are not called for. Relevant cases, such as micro aerial vehicles and very small aerial vehicles are receiving increased attention. A small plant can personally supply the solid aerodynamic information requisite to design this kind of aircraft: with oversized models, even at low test speeds, the same Reynolds number of the real aircraft can be secured.

Acknowledgment

The test phase of this research was carried out with the whirling arm equipment of the Fluid Dynamics Study Center of the Centro Nazionale Delle Ricerche (CNR).

References

[1]Beyers, M. E., "SDNM Pitch and Yaw Axis Stability Derivatives," AIAA Paper 85-1827, Aug. 1985.

[2]den Boer, R. G., and Cunningham, A. M., Jr., "Low-Speed Unsteady Aerodynamics of a Pitching Straked Wing at High Incidence—Part I: Test Program," *Journal of Aircraft*, Vol. 27, No. 1, 1990, pp. 23–30.

[3]Cunningham, A. M., Jr., and den Boer, R. G., "Low-Speed Unsteady Aerodynamics of a Pitching Straked Wing at High Incidence—Part II: Harmonic Analysis," *Journal of Aircraft*, Vol. 27, No. 1, 1990, pp. 31–41.

[4]Hanff, E. S., "Applications of Half-Model Technique in Dynamic Stability Testing," AGARD LS 114, NASA Ames, May 1981.

[5]Beyers, M. E., "Direct Derivative Measurements in the Presence of Sting Plunging," *Journal of Aircraft*, Vol. 23, No. 3, 1986, pp. 179–185.

[6]Greenwell, D. I., "Frequency Effects on Dynamic Stability Derivatives Obtained from Small-Amplitude Oscillatory Testing," *Journal of Aircraft*, Vol. 35, No. 5, 1998, pp. 776–782.

[7]Working Group 16, *Cooperative Programme on Dynamic Wind Tunnel Experiments for Manoeuvering Aircraft*, AR-305, AGARD, 1996.

[8]O'Leary, C. O., and Rowthorn, E. N., "New Rotary Rig at RAE and Experiments on HIRM," *Aeronautical Journal*, Vol. 90, No. 900, 1986, pp. 399–409.

[9]Ericsson, L. E., and Reding, J. P., "Dynamic Support Interference in High-Alpha Testing," *Journal of Aircraft*, Vol. 23, No. 12, 1986, pp. 889–896.

[10]Ericsson, L. E., "Reflection Regarding Recent Rotary Rig Results," *Journal of Aircraft*, Vol. 24, No. 1, 1987, pp. 25–30.

[11]Ericsson, L. E., "Another Look at High-Alpha Support Interference in Rotary Tests," *Journal of Aircraft*, Vol. 28, No. 9, 1991, pp. 584–591.

[12]Ericsson, L. E., and Beyers, M. E., "Wind-Tunnel Aerodynamics in Rotary Tests of Combat Aircraft Models," *Journal of Aircraft*, Vol. 35, No. 4, 1998, pp. 521–527.

[13]Beyers, M. E., and Ericsson, L. E., "Implications of Recent Rotary Rig Results for Flight Prediction," *Journal of Aircraft*, Vol. 37, No. 4, 2000, pp. 545–553.

[14]Khrabrov, A., Kolinko, K., Miatov, O., Vinogradov, J., and Zhuk, A., "Using Oscillatory Conning Experimental Rig for Separation of Rotary and Unsteady Aerodynamic Derivatives," *Proceedings of the 18th International Conference on Instrumentation in Aerospace Simulation Facilities*, IEEE Publications, Piscataway, NJ, 1999, pp. 37.1–9.

[15]Ericsson, L. E., "Lateral Oscillations of Sting-Mounted Models at High Alpha," *Journal of Spacecraft and Rockets*, Vol. 27, No. 5, 1990, pp. 508–513.

[16]Mulkens, M. J. M., and Ormerod, A. O., "Measurements of Aerodynamic Rotary Stability Derivatives Using a Whirling Arm Facility," *Journal of Aircraft*, Vol. 30, No. 2, 1993, pp. 178–183.

[17]Gili, P., "The Sweep-Back Angle and the Aerodynamic Induction Like Wing Contributions to the Dihedral Effect," *Proceedings of the 19th Congress of the ICAS*, AIAA, Reston, VA, Vol. 3, 1994, pp. 2868–2878.

[18]Gili, P., "Dihedral Effect for Straight Tapered and Twisted Wings," *Proceedings of the 20th Congress of the ICAS*, AIAA, Reston, VA, Vol. 1, 1996, pp. 585–592.

[19]Gili, P. A., "All of the Wing Contributions to C_{l_β} Evaluation," *Proceedings of the AIAA Atmospheric Flight Mechanics Conference*, AIAA, Reston, VA, 1997, pp. 70–81.

[20]Anderson, R. F., "Determination of the Characteristics of Tapered Wings," NACA TR 572, 1936.

[21]Guermond, J. L., "A Generalized Lifting Line Theory for Curved and Swept Wings," *Journal of Fluid Mechanics*, Vol. 211, No. 2, Feb. 1990, pp. 497–513.

[22]Queijo, M. J., "Theoretical Span Load Distributions and Rolling Moments for Side-Slipping Wings of Arbitrary Planform in Incompressible Flow," NACA TR 1269, 1956.

[23]Queijo, M. J., "Theory for Computing Span Loads and Stability Derivatives Due to Sideslip, Yawing and Rolling for Wings in Subsonic Compressible Flow," NASA TN D-4929, Dec. 1968.

[24]Javed, M. A., and Hancock, G. J., "Application of the Vortex Lattice Methods to Calculate L_v (Rolling Moment Due to Sideslip)," *Aeronautical Journal*, Vol. 85, No. 842, 1981, pp. 113–117.

[25]Miranda, L. R., Elliot, R. D., and Baker, W. M., "A Generalized Vortex Lattice Method for Subsonic and Supersonic Flow Applications," NASA CR 2865, 1977.

[26]Abbott, I. H., and Von Doenhoff, A. E., *Theory of Wing Sections*, Dover, New York, 1959, p. 256.